Analysis of Passive Islanding Detection Techniques for Double Line Fault in Three Phase Microgrid System

Bangar Raju LINGAMPALLI, Subba Rao KOTAMRAJU

Department of Electrical & Electronic Engineering, Koneru Lakshmaiah Educational Foundation, Greenfields, 522502 Vaddeswaram, Andhra Pradesh, India

lsmlbr@yahoo.in, principal.coe@kluniversity.in

Abstract. *Microgrids are able to dispatch power to distribution systems with the advancement of power electronics-based inverters. As per IEEE-1547-2018 standards, Microgrid has to maintain voltage of $0.88 \leq V \leq 1.1$ p.u (per unit) and frequency of $58.8 \leq f_0 \leq 61.2$ Hz and detect un-intentional faults in less than 2 seconds to bring Microgrid into islanding mode seamlessly. Unless these faults are detected and Microgrid is islanded, the system stability cannot be maintained and Microgrid cannot feed the connected loads. To detect these unsymmetrical faults, to bring the Microgrid to islanding mode and to be stable during non-islanding cases like loads switch on and throw off at Point of Common Coupling (PCC), a passive islanding detection method, Rate of Change of Voltage Phase Angle (ROCOVPA) is proposed. The methodology is simple. First, the voltage phase angle of generator bus and the grid is monitored. Then, absolute value is found and finally differentiated to get ROCOVPA and detect islanding. Also, this technique is compared with the widely used method of Rate of Change of Frequency (ROCOF) at different percentage active and reactive power mismatches. It also avoids nuisance tripping so that Microgrid's stability is maintained. This method is tested for un-symmetrical double line fault, for islanding cases and switch on or throw off, for non-islanding cases with linear and non-linear loads. In this method, the power quality is also not affected because of no perturbations during testing and the Non-Detection Zone (NDZ) is almost zero. The proposed method is verified by simulating islanding and non-islanding conditions in MATLAB/Simulink and by comparing with ROCOF method and found effective.*

Keywords

Distributed Generation, Line to Line fault, Non-Detection Zone, Point of Common Coupling, Rate of Change of Frequency, Rate of Change of Voltage Phase Angle.

1. Introduction

The normal operating mode of the Microgrid is in connection with the main grid or utility grid. In grid-connected mode, the Microgrid controller is in constant current mode, supplying power to load and importing mismatched power from the grid. But in islanded mode, the Microgrid controller has to maintain the voltage and frequency at PCC and supply power to load [1].

During grid-connected mode, the mismatched power is supplied by the grid and hence, the demand and supply are balanced. But in islanded mode, the Distributed Generator (DG) has to solely take care of the load. When islanding occurs at low or 0 % power mismatch, the condition can not be identified by the widely used relays like ROCOF as the variations are very low for the relay to send trip signal to circuit breaker and hence, the formation of NDZ. However, ROCOVPA can detect even those small variations and trip circuit breaker when islanding scenario is identified. It acts aptly for the islanding condition and isolates the Microgrid from the main grid in less than 2 seconds at 0 % NDZ [2], which meets IEEE-1547-2018 standards.

The un-intentional un-symmetrical fault considered for simulation in MATLAB/Simulink is double line (L-L) fault [3], [4] and [5]. Unless these faults are isolated, the safety and security of the equipment and staff are not taken care of. ROCOVPA is well suited for the detection of these un-intentional un-symmetrical faults and brings the Microgrid to autonomous mode seamlessly. The nuisance tripping is also avoided as ROCOVPA promptly differentiates islanding and non-islanding according to results of analysis. The stability of the network is also maintained without nuisance tripping and there is no power interruption to loads.

There are many islanding detection methods such as passive, active, hybrid, and communication types [6] and [7]. These are basically classified as local and remote methods based on control philosophy. All the passive, active, and hybrid methods utilize the local measurement of parameters like voltage, current, frequency, or active and reactive powers at PCC [8]. However, the remote methods utilize communication techniques as the networks are located far off from each other.

As per literature, all the passive islanding detection methods leave behind a considerable NDZ (percentage power mismatch), in which the islanding detection fails [9]. The active methods deteriorate the quality of power due to perturbations during testing which is subjected to nuisance tripping [10]. The communication methods are a bit costly and depend on the size of the Microgrid and the criticality of loads. To obviate all these issues, a passive islanding detection method is proposed for the small DG of 2.5 kW. It is designed and developed in MATLAB for testing as per UL-1741. Finally, the proposed method proved to be working well for the islanding and non-islanding cases based on the simulation results obtained in MATLAB/Simulink.

In this paper, the passive islanding detection technique, ROCOVPA is used for inverter interfaced DGs, for detecting un-symmetrical L-L-Fault and compared with widely used ROCOF, in MATLAB/Simulink. The proposed method measures the variation of voltage phase angles at different buses like grid and DG. Then, the absolute value of differential angle is calculated from PMU data and differentiated to get ROCOVPA for the confirmation of islanding or non-islanding event. This paper is organized as follows, Sec. 2. discusses the mathematical network model and MATLAB/Simulink model. Section 3. discusses the NDZ reduction. Section 4. presents the proposed method. Section 5. presents the inverter simulation parameters. Section 6. discusses the performance results of the Microgrid with the proposed methodology in MATLAB/Simulink with different percentage power mismatches. The last Sec. 7. concludes this paper and suggests future work on this research topic.

2. Mathematical Model of Network

The network model is shown in Fig. 1(a). The ROCOVPA islanding detection method is tested on a DG with 2.5 kW and an interfaced inverter. A parallel connected RLC (Resistive, Inductive and Capacitive) load is connected to DG with a quality factor of 1.8 at PCC. The DG inverter is connected to main grid via PCC through a 3-phase circuit breaker. The inverter is connected to PCC through a low pass filter.

(a) ROCOVPA testing circuit.

(b) NDZ circuit.
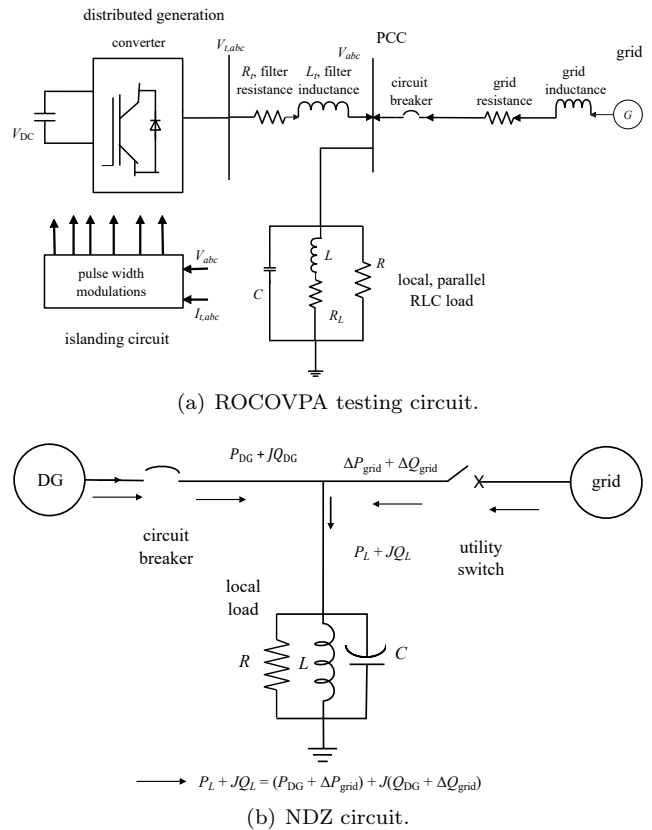
Fig. 1: Simple circuit of network for (a) testing the islanding detection method of ROCOVPA, (b) DG Network connected with Grid System to find NDZ.

The mathematical model of the islanded Microgrid in abc frame is given by the following equations:

$$V_{t,abc} = L_t \frac{d}{dt} i_{t,abc} + R_t i_{t,abc} + V_{abc}, \qquad (1)$$

$$i_{t,abc} = \frac{V_{abc}}{R + i_{L,abc}} + C \frac{d}{dt} V_{abc}, \qquad (2)$$

$$V_{abc} = V_L \frac{d}{dt} i_{L,abc} + R_L i_{L,abc}, \qquad (3)$$

where $V_{t,abc}$, $i_{t,abc}$, $i_{L,abc}$ are terminal 3-phase voltages and currents and V_{abc} is PCC voltage.

These three-phase instantaneous voltages and currents are to be transformed to synchronous rotating frame $dq0$, due to the following reasons:

- to have control of active power (d-axis) and reactive power (q-axis),

- to keep mutual inductance constant,

- to achieve the desired output,

- to have infinite gain control on Proportional Integral (PI), Proportional Integral Differential (PID), by adjusting integrators,

- to make steady-state error zero,

- to make computations easy.

$$\dot{\vec{X}}(t) = \mathbf{A}\vec{X}(t) + \vec{B}u(t), \tag{4}$$

$$y(t) = \vec{C}\vec{X}(t), \tag{5}$$

$$u(t) = V_{td}. \tag{6}$$

The $\mathbf{A}$, $\vec{B}$, $\vec{C}$ and $\vec{D}$ constants are given by:

$$\mathbf{A} = \begin{pmatrix} \dfrac{-R_t}{L_t} & \omega_0 & 0 & \dfrac{-1}{L_t} \\ \omega_0 & \dfrac{-R_t}{L_t} & -2\omega_0 & \left(\dfrac{R_l C \omega_0}{L} - \dfrac{\omega_0}{R}\right) \\ 0 & \omega_0 & \dfrac{-R_l}{L} & \left(\dfrac{1}{L} - \omega_0^2 C\right) \\ \dfrac{1}{C} & 0 & \dfrac{-1}{C} & \dfrac{-1}{RC} \end{pmatrix}, \tag{7}$$

$$\vec{B}^T = \left(\dfrac{1}{L_t}, 0, 0, 0\right), \tag{8}$$

$$\vec{C} = (0, 0, 0, 1), \tag{9}$$

$$\vec{D} = (0, 0, 0, 0), \tag{10}$$

$$\vec{X}^T = (i_{td}, i_{tq}, i_{Ld}, v_d). \tag{11}$$

These equations give the transfer functions of V_d / V_{td}, where V_d and V_{td} are input and output components of d-axis.

3. Non-Detection Zone

The islanding detection depends on two factors:

- NDZ – Non-Detection Zone, which is as per IEEE-1547, must be < 15 % of power mismatch [11],

- type of the load [12].

The DG network is connected with the grid as shown in Fig. 1(b). In grid-connected mode, utility supplies the mismatched power between DG and the load and maintains the voltage V and frequency f at PCC [13]

and [14]. If ΔP and ΔQ are mismatches of active and reactive powers supplied by utility to load:

$$P + \Delta P = \frac{v^2}{R}, \tag{12}$$

$$Q + \Delta Q = \frac{v^2}{2\pi f L}. \tag{13}$$

From the above, the voltage and frequency at PCC is given by:

$$V = \sqrt{R(P + \Delta P)}, \tag{14}$$

$$f = \frac{v^2}{2\pi L(Q + \Delta Q)}. \tag{15}$$

However, under islanding conditions, the Microgrid is brought to isolated mode from grid. The Under/Over Voltage Protection (UVP/OVP) and Under/Over Frequency Protection (UFP/OFP) methods are very simple and incorporated in all grid-connected inverters and relays connected with DG system protection. In these methods, the voltage and frequency are both constantly monitored at PCC where:

$$\Delta P = P_{\text{LOAD}} - P_{\text{DG}}, \tag{16}$$

$$\Delta Q = Q_{\text{LOAD}} - Q_{\text{DG}}, \tag{17}$$

If $\Delta P = 0$, then voltage at PCC will fluctuate off normal level. Similarly, if $\Delta Q = 0$, then frequency at PCC will fluctuate off normal level, which is an indication of islanding condition. However, both these islanding detection methods leave behind a large Non-Detection Zone (NDZ). The islanding detection may fail, when the mismatch ΔP and ΔQ are close to zero. When ΔP and ΔQ become zero, the voltage V' and frequency f' under islanding mode are given by:

$$V' = \sqrt{R(P)}, \tag{18}$$

$$f' = \frac{v'^2}{2\pi L(Q)} = \frac{R(P)}{2\pi L(Q)}. \tag{19}$$

Then, the voltage and frequency deviations due to power mismatch are given by:

$$\Delta V = V' - V = \sqrt{R(P)} - \sqrt{R(P + \Delta P)}, \tag{20}$$

$$\Delta f = f' - f = \frac{v'^2}{L(Q)} - \frac{V'^2}{L(Q + \Delta Q)} = \\ = \frac{R \cdot P}{L \cdot Q} - \frac{R(P + \Delta P)}{L(Q + \Delta Q)}. \tag{21}$$

The above two equations show that the variations in voltage and frequency occur due to power mismatch. If the power mismatch is substantial, the variations in voltage and frequency can be identifiable. If the mismatch is too small, leading to less than 15 %, the islanding cannot be detected and hence, the NDZ cannot be formed. Figure 1(b) shows the NDZ for different percentage power mismatches.

When the reference value is 88 % and 110 % (see Tab. 1) for under/over voltage and grid RMS Voltage $V_g = 415$ V, then $V_{max} = 456$ V, $V_{min} = 365$ V. The schematic diagram of the grid-connected Microgrid is shown in Fig. 2(a). The inverter gate pulses take the feedback grid voltage and the set reference. The trigger pulses are sent to inverter accordingly and the output voltage is controlled. The PV is connected to buck/boost converter to have control on DC reference voltage. The DC/DC Converter is connected to interfacing inverter. The inverter is connected to PCC via a low pass filter LCL. The Microgrid is connected to the grid via a circuit breaker, so that the Microgrid can be islanded during faults in the system. A local parallel RLC load with high quality factor is connected to the Microgrid at PCC and the Microgrid feeds this local load from DG, even in the absence of a grid.

V_{ref} – voltage reference; V_{pcc} – voltage at PCC; V_g – voltage of grid; LCL – low pass filter;

I_{ref} – current reference; I_{pcc} – current at PCC; I_g – current of grid;

(a) Microgrid diagram.

(b) NDZ mapping.
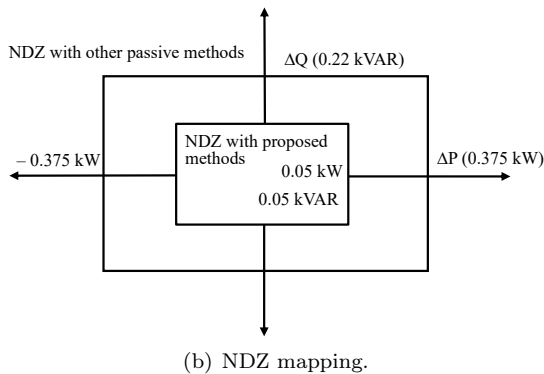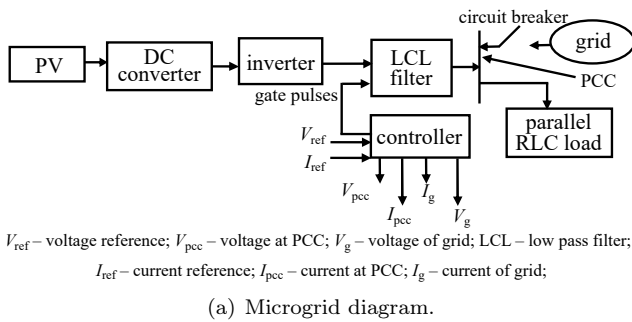
Fig. 2: (a) Schematic diagram of the grid connected to the Microgrid, (b) mapping of the NDZ in ΔP versus ΔQ for Over/Under Voltage and Over/Under Frequency Relays.

The NDZ is the operating region [15] in which islanding detection methods cannot detect islanding as specified by IEEE-1547 standards. It is expressed in terms of percentage power mismatch or of the parameters like R, L, and C of the load. An approximate representation of the NDZ in terms of active and reactive power is given in this section. The NDZ of OVP/UVP and OFP/UVP islanding schemes are shown in Fig. 2(b). These methods fail to detect islanding when a power mismatch is less than 15 %. In distribution network, voltage and frequency values, as per standards are from 0.88 V to 1.1 V p.u for voltage relays and from 49 Hz

to 51 Hz for frequency relays [16] and [17]. These voltage and frequency levels are between 365–456 V and 49–51 Hz respectively (for a 3-phase, 415 V, 50 Hz system). The calculated active and reactive power mismatches for our test network (for the inverter rated output power of 2.5 kW and 1.48 kVAR) are ±0.375 kW and ±0.22 kVAR, respectively.

In grid mode, load consumes the reactive power [18] and [19]. But in islanding, DGs can not inject reactive power to load, as DGs operate at unity power factor, because load behaves like resistance as the load resonance frequency is equal to system frequency at PCC [20], [21] and [22]. Hence, to find more deviations in frequency, the load selected is parallel RLC with a high quality factor of 1.8 in islanding mode [23], [24] and [25]. The quality factor Q_f is given by:

$$Q_f = \omega_0 RC = \frac{R}{\omega_0 L} = R\sqrt{\frac{C}{L}}, \qquad (22)$$

where $\omega_0 = 2\pi f_0 = \frac{1}{\sqrt{LC}}$.

High-quality factor loads have high capacitance and small inductance with or without high parallel resistance [26], [27], [28] and [29]. The islanding detection is complex with resonant frequency loads of higher quality factor. The percentage mismatch is not the criterion for load parameters [30] and [31]. The load reactive power is given by:

$$Q_{LOAD} = V_{rms}^2 \left(\frac{1}{\omega L} - \omega c \right) = \Delta Q. \qquad (23)$$

Equation (23) depicts the variation in reactive power for different values of L and C [32] and [33]. The percentage mismatch powers for OVP/UVP and OFP/UFP relays are shown in Fig. 2(b) and are given by Eq. (24) and Eq. (25) for active and reactive power imbalances respectively,

$$\Delta P = 3V \cdot I - 3(V + \Delta V) \cdot I = -3V \cdot \Delta V \cdot I, \quad (24)$$

where V and I are rated voltage and current of the system. The islanding standards are shown in Tab. 1. As per IEEE-1547-2018 standards, voltage range for threshold is of $0.88 \leq V \leq 1.1$ p.u. and frequency range for 60 Hz is of $58.8 \leq f_0 \leq 61.2$ Hz [34] and [35].

The frequency range as per IEEE-1547-2018 is between 49 and 51 Hz for a 50 Hz Microgrid and the voltage is between 365 and 456 V for a nominal voltage of 415 V and the parameter $\Delta V = V' - V$ range is not considered as the case of zero power mismatch is considered [36]. Also, the comparison of ROCOVPA and ROCOF is done in MATLAB/Simulink at various power mismatches. In this case, the voltage fluctuations will not cross the limits. But in other cases, when load active power $P_L >$ generated active power

Tab. 1: Islanding standards.

Standard	Detection time (s)	Quality factor	Trip frequency range, nominal frequency f_0 (Hz)	Trip voltage range (V)
IEC 62116	$t < 2$	1	$f_0 - 1.5 \leq f \leq f_0 + 1.5$	$0.88 \leq V \leq 1.15$
Korean	$t < 0.5$	1	$59.3 \leq f_0 \leq 60.5$	$0.88 \leq V \leq 1.10$
IEEE-1547-2018	$t < 2$	1	$58.8 \leq f_0 \leq 61.2$	$0.88 \leq V \leq 1.10$
IEEE-929-2000	$t < 2$	2.5	$59.3 \leq f_0 \leq 60.5$	$0.88 \leq V \leq 1.10$

P_G (+15 %) or $P_L < P_G$ (−15 %), the voltage suddenly goes down or up, respectively.

$$\Delta G = 3\frac{v^2}{\omega_n L}\left(1 - \omega^2 LC\right) = 3\frac{v^2}{\omega_n L}\left(1 - \frac{\omega_n^2}{\omega_r^2}\right), \quad (25)$$

where ω_n and ω_r are system and resonance frequencies. The system frequency varies till it reaches resonant frequency of the load in islanding mode and is given by:

$$\omega_R = \frac{1}{\sqrt{LC}}, \quad (26)$$

and the reactive power imbalance is given by:

$$\Delta G = 3\frac{v^2}{\omega_n L}\left(1 - \frac{f_n^2}{f_n \pm \Delta f^2}\right). \quad (27)$$

According to the above derivations, ΔP affects the voltage and ΔQ affects the frequency during the islanding condition, which is tested in this paper in the simulation sections.

4. Proposed Methodology of Islanding Detention

This paper discussed a passive islanding detection method with negligible NDZ, which utilizes the PLL signals of the inverter of the DG. During islanding mode, there is variation of voltage phase angle at PCC. In this technique, the voltage phase angle is measured at the specified DG terminals and then the ROCOVPA is calculated. In non-islanding mode, the rate of change of phase angle becomes negligible after some time. On contrary, in islanding mode, this change in voltage phase angle is sufficient enough for the islanding condition to be detected after some time. This measurement is used to isolate DG from utility grid. It is also pertinent to note that the nuisance tripping is avoided, retaining the stability of the system. Thus, this passive islanding detection proved to be better than other methods like Rate of Change of Frequency (ROCOF), Rate of Change of Voltage over Active Power (ROCOVP), Rate of Change of Active Power (ROCAP), Rate of Change of Reactive Power (ROCORP) etc.

The combined MATLAB model used for estimating the islanding detection of both ROCOVPA and ROCOF is shown in Fig. 3(a).
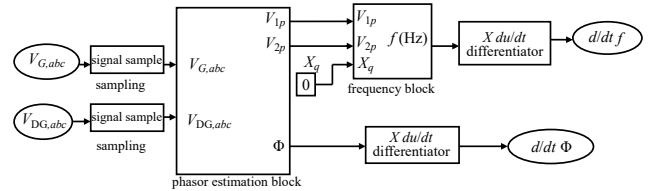
(a) Phasor estimation block.
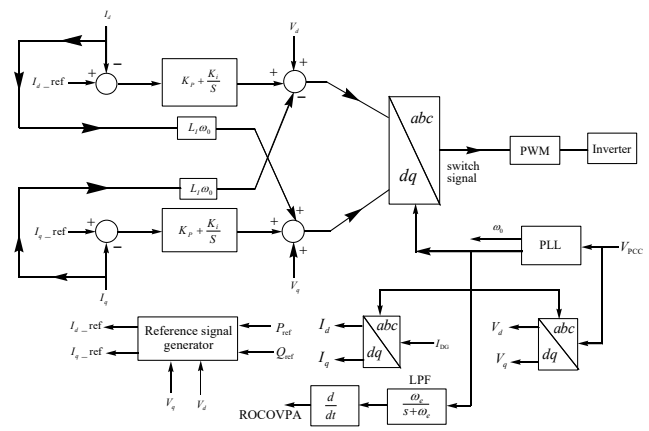
(b) Current controller.

Fig. 3: (a) Phasor estimation block for computing islanding of ROCOVPA and ROCOF. V_G (V1) is grid side voltage and V_{DG} (V2) is DG side voltage reference. (b) Current controller block diagram.

The proposed method is tested with the 2.5 kW DG with current control mode interfacing inverter connected to an RLC load with 1.8 quality factor. Figure 3(b) shows the current control mode to control active and reactive power of load and the islanding detection of Microgrid with DG, with the proposed method of ROCOVPA.

In the proposed method, the variation of ROCOVPA is monitored at DG bus and grid bus. If there is change in the voltage phase angle, the rate with respect to time is calculated. During the islanding, the deviations of the rate of change of phase angle is high enough and hence the islanding is detected. If the relay threshold is fixed, then the trip command to circuit breaker is initiated during fault conditions, when the threshold crosses the limit.

The algorithm for the flow chart of ROCOVPA method of islanding detection is shown in Fig. 4.
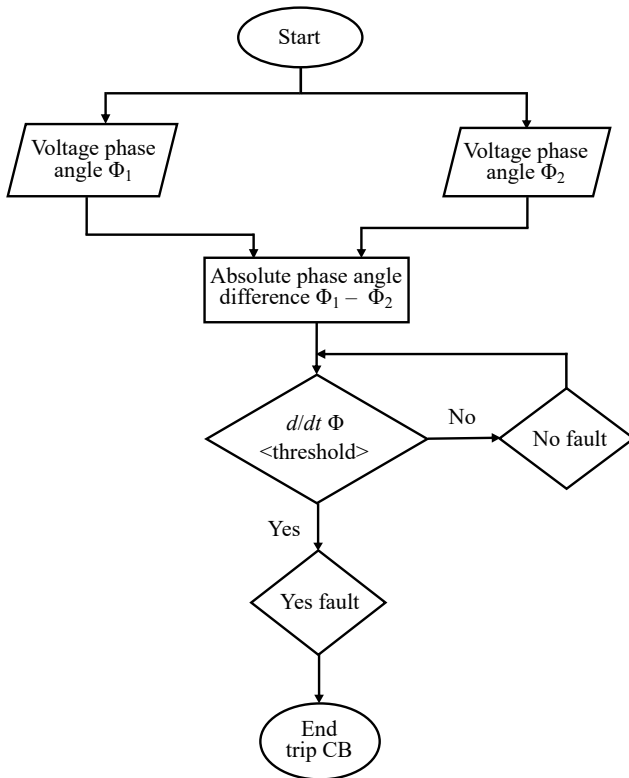
Fig. 4: Flow chart of the proposed ROCOVPA for the islanding detection.

Tab. 2: Inverter parameters for simulation.

Component	Value and units
DG power	2.5 kW
Switching frequency	10 kHz
DC input voltage	500 V
Line voltage	415 V
Filter capacitance C_f	2 µF
Filter inductance L_f	5 mH
Damping resistance R_f	10 Ω
Nominal frequency	50 Hz
Load resistance R_L	1.76 mΩ
Load inductance L_L	3.2 mH
Load capacitance C_L	3.2 µF
Load quality factor $\left(Q = R\sqrt{\frac{C}{L}}\right)$	1.8
Load resonant freq. $\left(f_r = \frac{1}{2\pi\sqrt{LC}}\right)$	50 Hz
Current controller proportional gain k_p	0.4
Current controller integral gain k_i	500

4.1. Algorithm for ROCOVPA

The flow diagram of ROCOVPA is explained in the Fig. 4. Voltage at DG side / PCC is measured and the voltage phase angle is extracted. After measurement of phase angle of voltage, the rate of change of voltage phase angle is calculated. In a normal situation, this value is lower than 1 deg·s^{-1} but during islanding condition, the value suddenly increases to more than 2 deg·s^{-1} variation depending on the fault severity, by means of which the islanding is detected. During non-islanding mode, this value is in threshold limit and hence, nuisance tripping is avoided.

5. Inverter Parameters for Simulation

The method based on ROCOVPA proposed in this paper is shown in Fig. 1 and the used parameters are shown in Tab. 2.

The DG capacity with interfaced inverter is 2.5 kW. The interfaced inverter is connected to main grid through a breaker via PCC. A 3-phase parallel RLC load is connected at PCC. The input DC Voltage to the inverter is 500 V. The output line to line voltage of inverter is 415 V. The line resistance and inductance are 1.5 mΩ and 2 mH, respectively. The nominal grid frequency is 50 Hz. The inverter switching frequency is set as 10 kHz. The load parameters with a quality factor of 1.8 are $R_L = 1.76$ mΩ, $L_L = 3.2$ mH and $C_L = 3.2$ µF. The load resonant frequency is 50 Hz. Current controller gains are $K_p = 0.4$ and $K_i = 500$. All these parameters are shown in Tab. 2. Constant current control technique is used to regulate the frequency and voltage at PCC. The normal PLL is used for synchronizing DG to the grid. PWM control takes the feedback from PCC to regulate voltage, frequency, and power. The controller basically takes into account the local measurements only and this is a three-phase AC Microgrid. During grid mode, voltage and frequency are maintained by the grid but in islanding mode, the frequency, voltage, and power are controlled by inverter controller. In islanding, the reverse droop characteristic principle of frequency proportional to reactive power and voltage proportional to active power is applicable.

6. Results Analysis and Discussion

The designed network is tested in MATLAB/Simulink for islanding cases of un-intentional un-symmetrical L-L fault and non-islanding cases of switch on and disconnection of linear load. The MATLAB Simulation results of ROCOVPA and ROCOF are compared. It is proved that ROCOVPA is better than ROCOF.

6.1. Analysis of Different Islanding Cases for Un-symmetrical L-L Fault in the System

An un-symmetrical L-L fault is initiated in the system at PCC at 0.4 s in MATLAB Simulink at 0 % power mismatch. $P_L = P_G$ is the condition for 0 % power mismatch and at that load, a L-L fault is initiated on the grid side at 0.4 s. The simulation graph is shown in Fig. 5(a). The proposed ROCOVPA detected islanding within 20 ms and a fixed threshold of 2 deg·s^{-1}. The relay can exactly detect and send a command to trip the circuit breaker to bring the Microgrid into islanding mode from grid mode. The total time is the sum of relay time and breaker time. Any type of the fault is to be cleared within 4 cycles (2 cycles, i.e., 0.04 s of relay operation + 2 cycles, 0.06 s of breaker operation). Hence, the ROCOVPA can detect the fault condition and island the Microgrid in around 1 s by tripping the circuit breaker, which is less than 2 s as per the standards of IEEE-1547-2018. The Microgrid testing is done as per UL-1741.

The same fault conditions are applied and tested with ROCOF in MATLAB as shown in Fig. 5(b) and the islanding is detected in 40 ms. If the threshold value is fixed at 0.02 Hz·s^{-1}, the tripping of the circuit breaker can be actuated in around 1 s which is below the standards of 2 s. The detection time of ROCOF is more than that of ROCOVPA. As the ROCOF is dependent on frequency, at lower percentage power mismatches, the threshold value cannot be fixed exactly. Hence, detection time varies inversely with percentage power mismatch.

To obviate all these issues, ROCOVPA is suggested and proved to be a better islanding detection method for un-symmetrical faults as described in Sec. 6. The MATLAB simulation results of both ROCOVPA and ROCOF are shown in Fig. 5(a) and Fig. 5(b).

6.2. Analysis of Different Non-islanding Cases with Linear load.

System stability has been studied for different transient conditions during linear and non-linear loads switch on and throw off at PCC with linear load for ROCOVPA and ROCOF in MATLAB/Simulink. Both ROCOVPA and ROCOF proved their stability by keeping within the threshold values to avoid nuisance tripping. The ROCOVPA threshold value is fixed at 2 deg·s^{-1} and that of ROCOF at 0.02 Hz·s^{-1}. The simulation results of ROCOVPA and ROCOF for the non-islanding cases with linear load are shown in Fig. 6(a) and Fig. 6(b).

The stability during the non-islanding operation of ROCOVPA and ROCOF during linear loads switch on and throw off at PCC is tested in MATLAB/Simulink. A linear resistive load is connected at PCC at 0.4 s and disconnected at 0.8 s. The variations of ROCOVPA and ROCOF show that the thresholds are much lower than 2 deg·s^{-1} and 0.02 Hz·s^{-1} respectively. Hence, the system is stable without any nuisance tripping of the circuit breaker and avoiding the islanding of the Microgrid.

6.3. Non-islanding Case with Non-linear Load Switch on and Throw off

The stability during the non-islanding operation of ROCOVPA and ROCOF during non-linear loads switch on at 0.4 s and throw off at 0.8 s at PCC is tested in MATLAB/Simulink. The nature of the non-linear loads selected is of resistive and inductive reactance type, so the variations will be higher. The results of non-islanding scenarios of ROCOVPA and ROCOF are shown in Fig. 7(a) and Fig. 7(b). The variations of ROCOVPA and ROCOF show that the thresholds are much lower than 2 deg·s^{-1} and 0.02 Hz·s^{-1} respectively. Hence, the system is stable without any nuisance tripping and power interruption to loads.

6.4. Analysis of Different Percentage Power Mismatches for L-L Fault on the System

In this section, different percentage power mismatches, both active and reactive, have been tested for L-L fault on ROCOVPA and ROCOF. The DG power selected in all percentage power mismatches is 2.5 kW. The 0 % power mismatch has already been tried, see Fig. 5(a) and Fig. 5(b), and the results obtained are 2 deg·s^{-1} at 20 ms for ROCOVPA and 0.02 Hz·s^{-1} at 40 ms. Herein, different active and reactive power mismatches such as 10 %, 15 %, and 20 % have been examined for both ROCOVPA and ROCOF relays. The detection time of ROCOVPA for 0 %, 10 %, 15 % and 20 % is consistent at 20 ms. But for ROCOF, the detection time is inversely proportional to percentage power mismatch. That is as the power mismatch is increasing in the case of ROCOF, the detection time is reducing, concluding that the detection time is less at a higher percentage power mismatch.

The graphs of 10 %, 15 % and 20 % for active power mismatch are shown in Fig. 8(a), Fig. 8(b), Fig. 9(a), Fig. 9(b), Fig. 10(a) and Fig. 10(b) for ROCOVPA (a) and ROCOF (b), respectively.

(a) ROCOVPA for L-L fault.
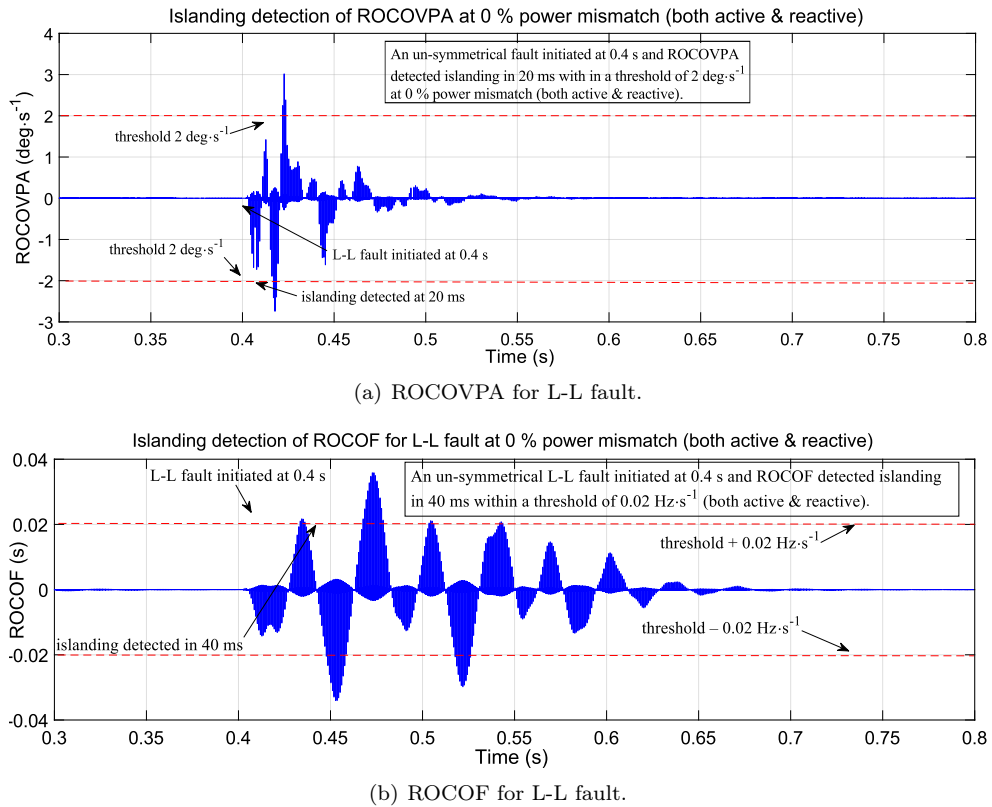
(b) ROCOF for L-L fault.

Fig. 5: (a) Islanding detection of ROCOVPA for L-L fault on the system, (b) islanding detection of ROCOF for L-L fault on the system.

(a) ROCOVPA for linear load.

(b) ROCOF for linear load.
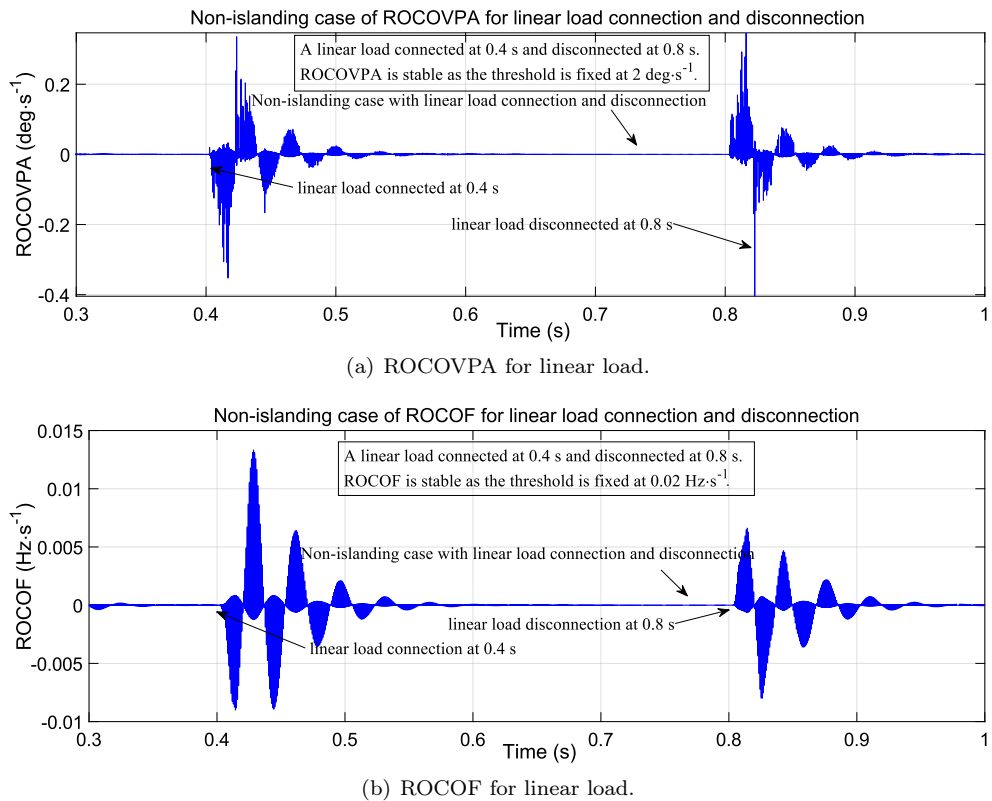
Fig. 6: (a) Non-islanding case of ROCOVPA for linear load switch on and throw off, (b) non-islanding case of ROCOF for linear load switch on and throw off.
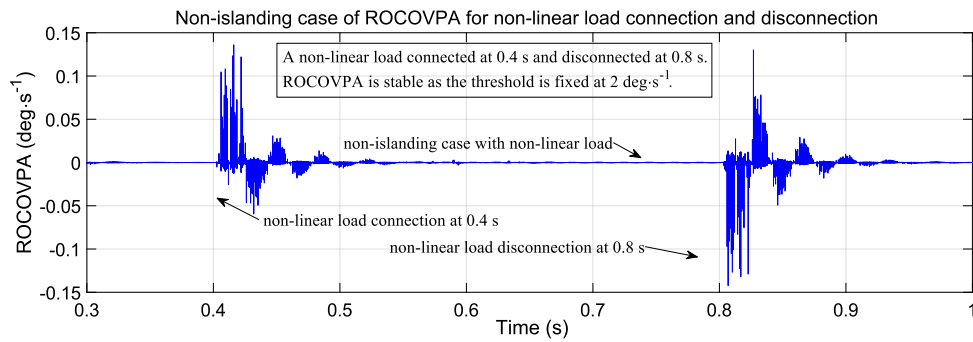
(a) ROCOVPA for non-linear load.
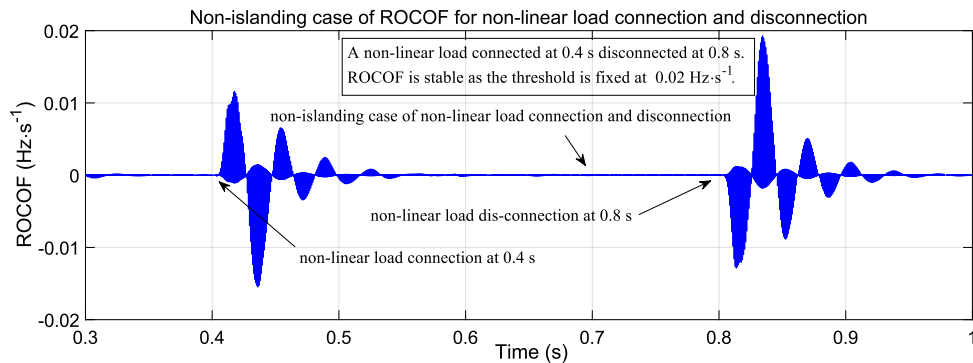
(b) ROCOF for non-linear load.

Fig. 7: (a) Non-islanding case of ROCOVPA for non-linear load switch on and throw off, (b) non-islanding case of ROCOF for non-linear load switch on and throw off.
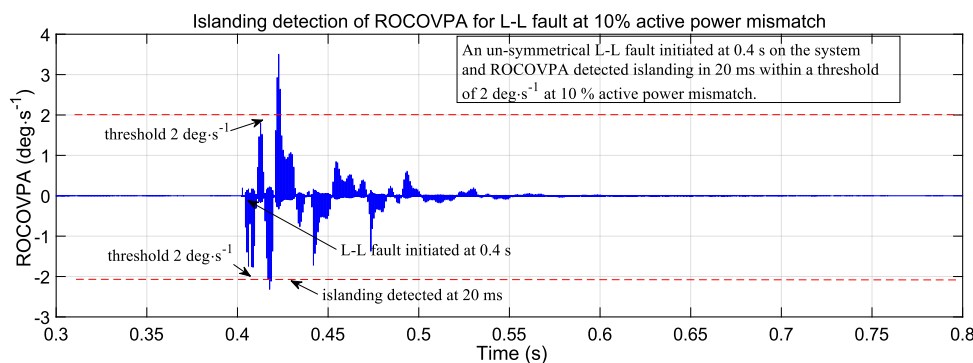
(a) ROCOVPA for L-L fault at 10 % active power mismatch.
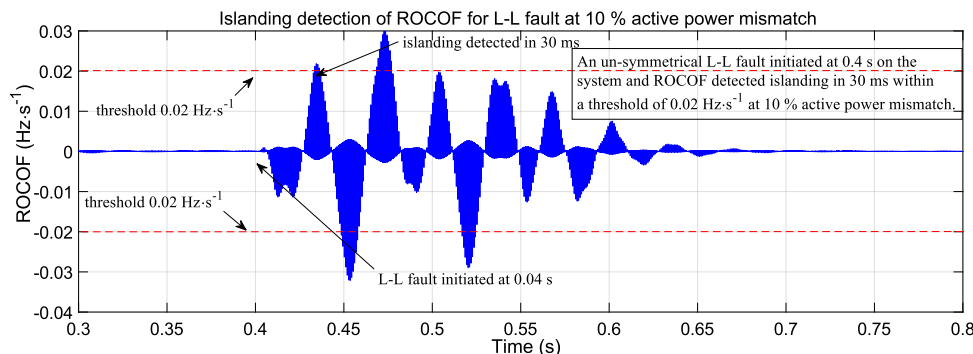
(b) ROCOF for L-L fault at 10 % active power mismatch.

Fig. 8: Islanding detection of (a) ROCOVPA for L-L fault at 10 % active power mismatch and (b) ROCOF for L-L fault at 10 % active power mismatch.

(a) ROCOVPA for L-L fault at 15 % active power mismatch.

(b) ROCOF for L-L fault at 15 % active power mismatch.

Fig. 9: Islanding detection of (a) ROCOVPA for L-L fault at 15 % active power mismatch and (b) ROCOF for L-L fault at 15 % active power mismatch.
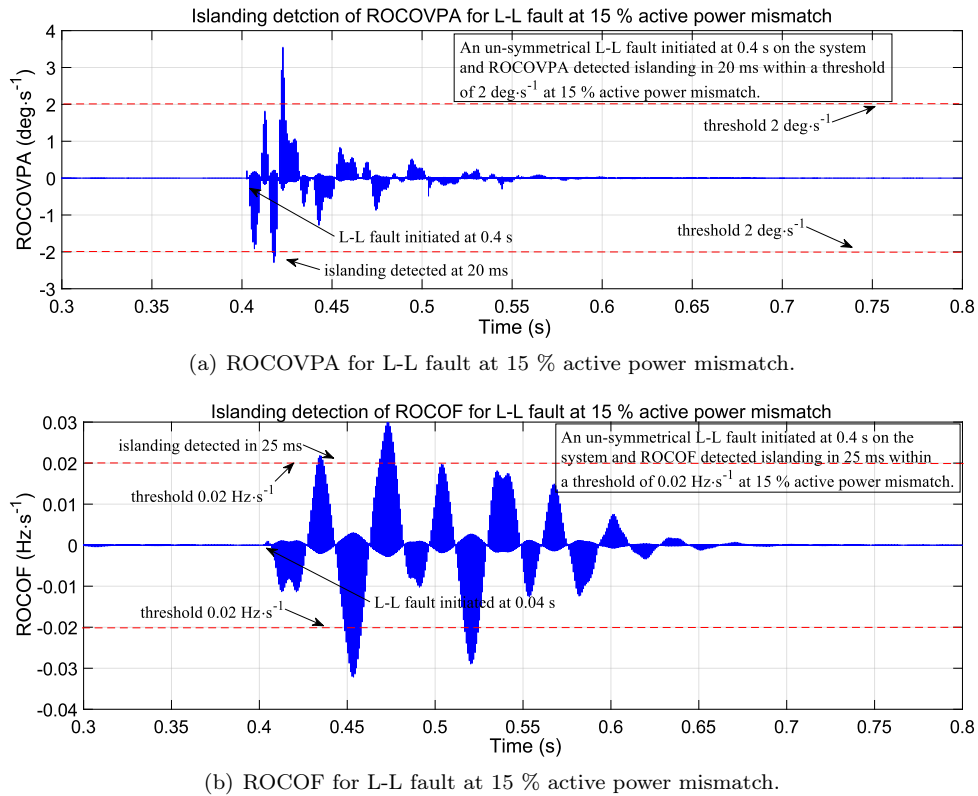
(a) ROCOVPA for L-L fault at 20 % active power mismatch.

(b) ROCOF for L-L fault at 20 % active power mismatch.

Fig. 10: Islanding detection of (a) ROCOVPA for L-L fault at 20 % active power mismatch and (b) ROCOF for L-L fault at 20 % active power mismatch.
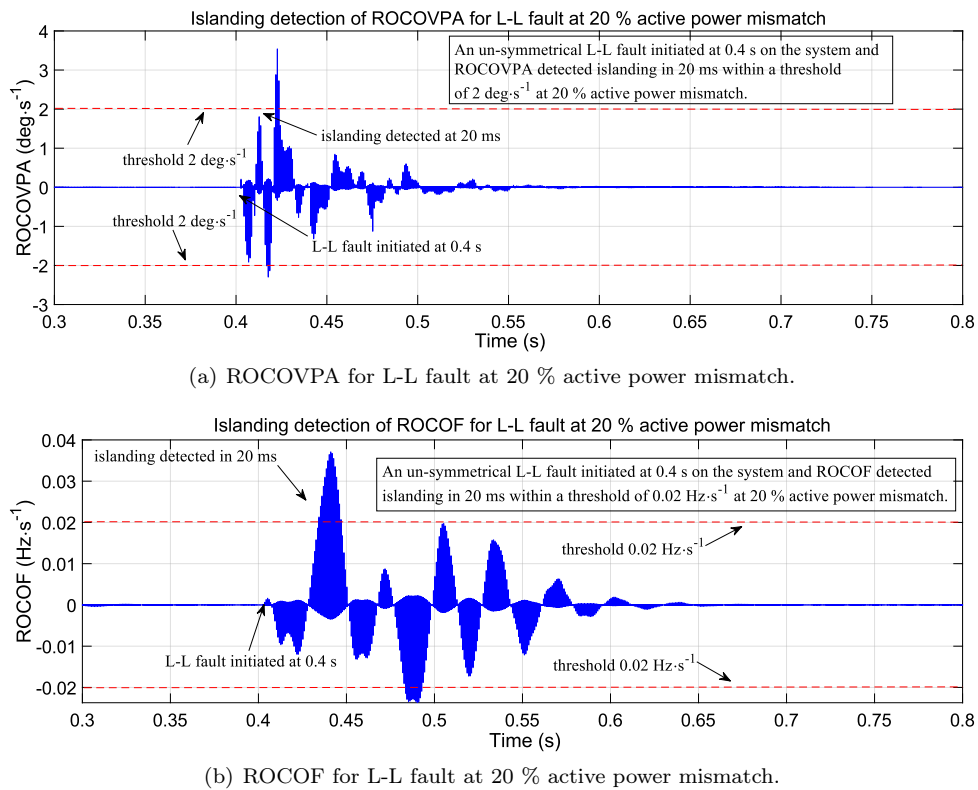
(a) ROCOVPA for L-L fault at 10 % reactive power mismatch.

(b) ROCOF for L-L fault at 10 % reactive power mismatch.
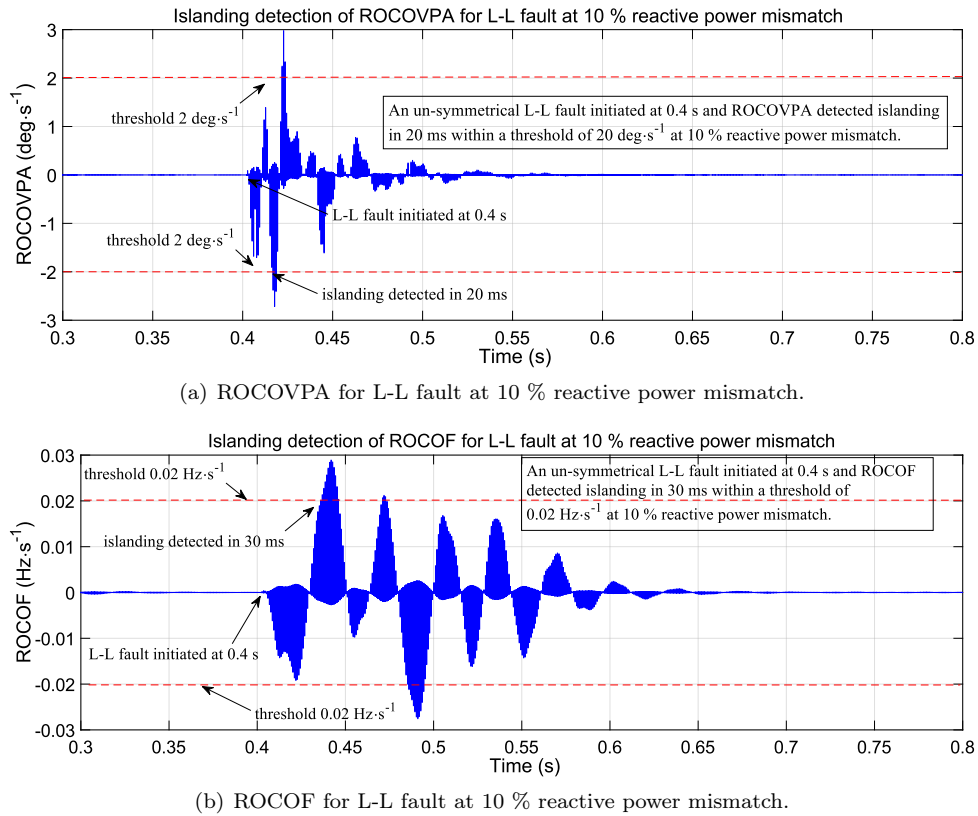
Fig. 11: Islanding detection of (a) ROCOVPA for L-L fault at 10 % reactive power mismatch and (b) ROCOF for L-L fault at 10 % reactive power mismatch.

Similarly, the graphs of reactive power mismatch of ROCOVPA and ROCOF for different reactive power mismatches of 10 %, 15 % and 20 % are shown in Fig. 11(a), Fig. 11(b), Fig. 12(a), Fig. 12(b), Fig. 13(a) and Fig. 13(b).

Also, active and reactive power mismatches vs time of 0 %, 10 %, 15 % and 20 % are shown in Fig. 14(a) and Fig. 14(b) respectively.

Table 3 gives the simulation results of detection times for different active power mismatches shown in Fig. 8, Fig. 9 and Fig. 10.

Tab. 3: Detection times of different percentage active power mismatches.

Active power mismatch	ROCOVPA detection time (ms)	ROCOF detection time (ms)
0 %	20	40
10 %	20	30
15 %	20	25
20 %	20	20

Table 4 gives the simulation results of detection times for different active power mismatches shown in Fig. 11, Fig. 12 and Fig. 13.

Tab. 4: Detection times of different percentage reactive power mismatches.

Reactive power mismatch	ROCOVPA detection time (ms)	ROCOF detection time (ms)
0 %	20	35
10 %	20	30
15 %	20	25
20 %	20	20

The graphs of detection times at different active and reactive power mismatches are drawn in Fig. 14(a) and Fig. 14(b).

7. Conclusion

In this paper, a Rate Of Change Of Voltage Phase Angle (ROCOVPA) method is proposed to detect unsymmetrical L-L fault in the three-phase Microgrid system with inverter interfaced DG. This method first monitors the phase angle between the DG bus and the grid bus. Then the absolute value of the phase angle is calculated and finally, this value is differentiated to get ROCOVPA to detect islanding or non-islanding. The variations in phase angle during fault conditions are sufficient enough to detect the islanding in 20 ms
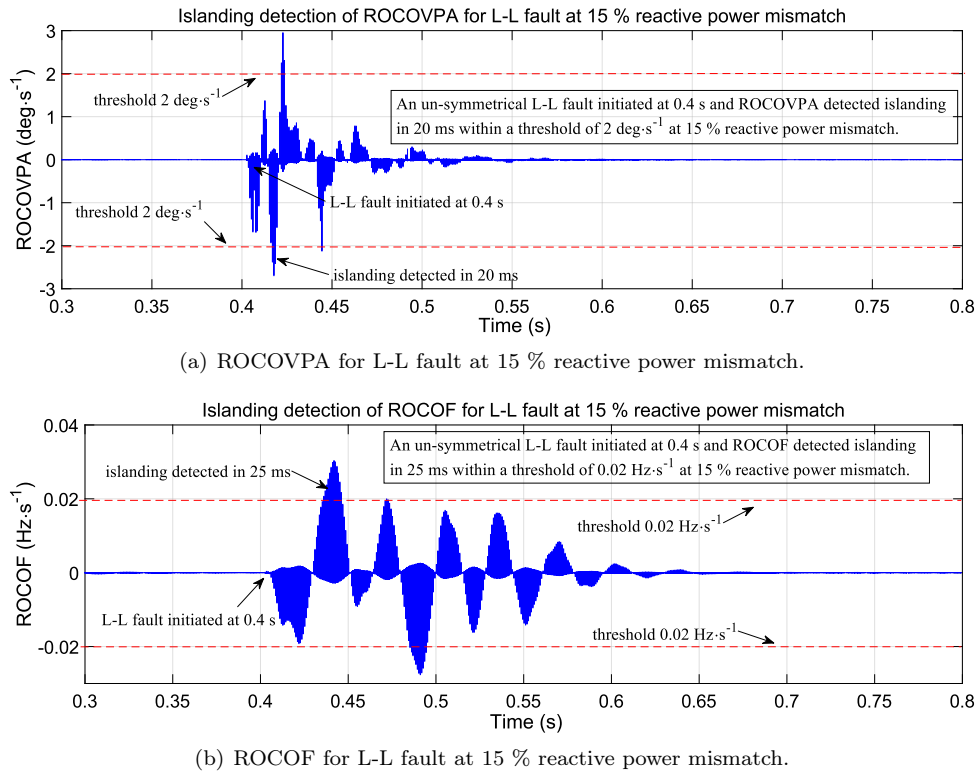
(a) ROCOVPA for L-L fault at 15 % reactive power mismatch.

(b) ROCOF for L-L fault at 15 % reactive power mismatch.

Fig. 12: Islanding detection of (a) ROCOVPA for L-L fault at 15 % reactive power mismatch and (b) ROCOF for L-L fault at 15 % reactive power mismatch.

(a) ROCOVPA for L-L fault at 20 % reactive power mismatch.

(b) ROCOF for L-L fault at 20 % reactive power mismatch.

Fig. 13: Islanding detection of (a) ROCOVPA for L-L fault at 20 % reactive power mismatch and (b) ROCOF for L-L fault at 20 % reactive power mismatch.
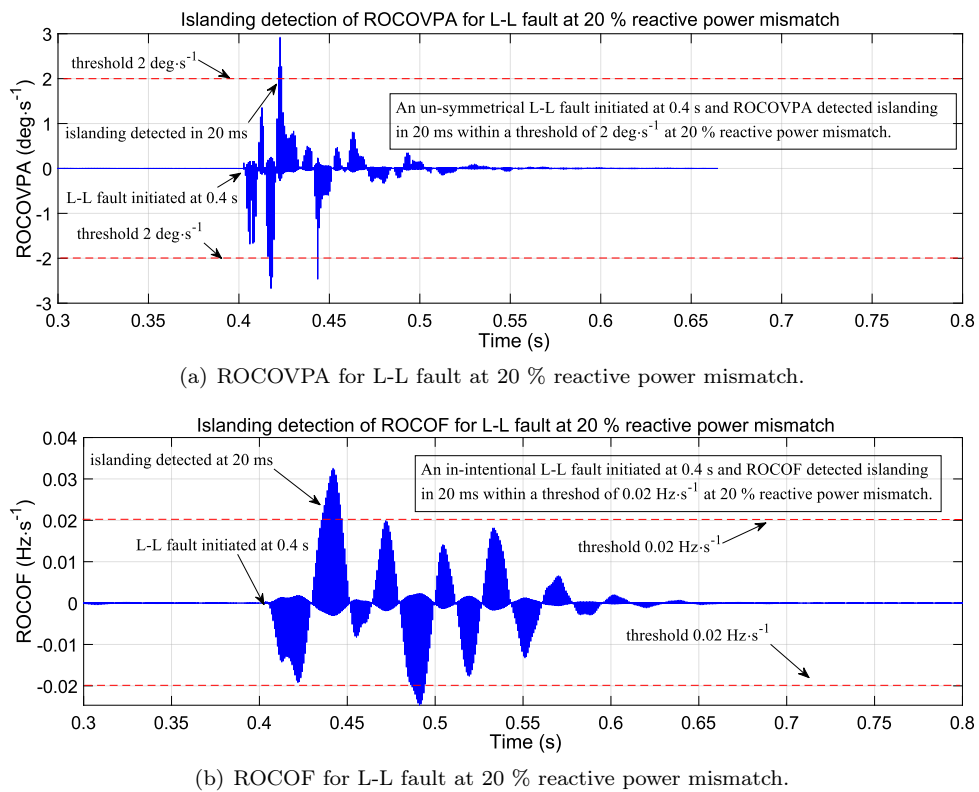
(a) ROCOVPA/ROCOF graphs for % active power mismatch vs time.

(b) ROCOVPA/ROCOF graphs for % reactive power mismatch vs time.
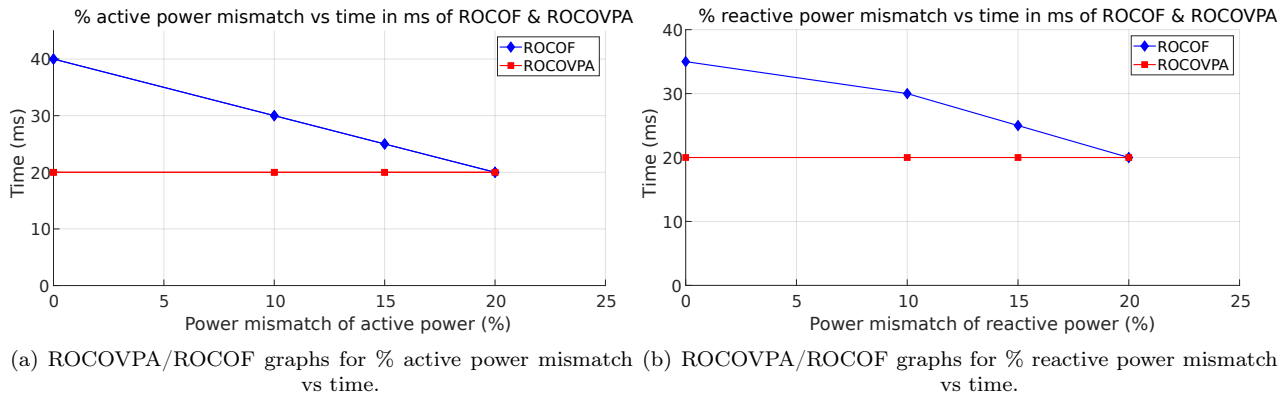
Fig. 14: (a) % active power mismatch vs time of defection, (b) % reactive power mismatch vs time of defection.

which is a very low period as compared to other methods. The proposed method gives the satisfactory results of islanding detection for un-symmetrical faults in the three-phase Microgrid and is stable for non-islanding cases like linear and non-linear loads switch on and throw off at PCC. It is proved with the MATLAB Simulation results in Sec. 6., that the proposed scheme is fast in detection time, reliable as it detects aptly the fault conditions and effective as it discriminates between islanding and non-islanding to avoid nuisance tripping. In the present technique, it is evident from the simulations, that the NDZ is almost negligible. It can also be concluded from the analysis of results, that ROCOVPA is a better method than ROCOF.

The future work can be extended with the same proposed technique of ROCOVPA with hybrid DGs, so that the power flow control with different inverter topologies can be applied for the stability of the Microgrid in islanded mode and for proportional load sharing.

Acknowledgment

Financial Disclosure

Author Contributions

B.R.L. developed the theoretical concept, performed analytical calculations and MATLAB simulations. Both the authors contributed to the final version of the manuscript. S.R.K. supervised the total project with a good number of suggestions.

References

[1] MILOSEVIC, D. and Z. DURISIC. Technique for stability enhancement of microgrids during un-symmetrical disturbances using battery connected by single-phase converters. *IET Renewable Power Generation*. 2020, vol. 14, iss. 9, pp. 1529–1540. ISSN 1752-1424. DOI: 10.1049/iet-rpg.2019.0625.

[2] KUMAR, D. A Survey on Recent Developments of Islanding Detection Techniques. *Turkish Journal of Electrical Power and Energy Systems*. 2021, vol. 1, iss. 1, pp. 42–53. ISSN 2791-6049. DOI: 10.5152/tepes.2021.21012.

[3] REDDY, C. R. and K. H. REDDY. Islanding detection for inverter based distributed generation with Low frequency current harmonic injection through Q controller and ROCOF analysis. *Journal of Electrical Systems*. 2018, vol. 14, iss. 2, pp. 179–191. ISSN 1112-5209.

[4] ELSHRIEF, Y., S. ABD-ELHALEEM, A. ABOZALAM and A. DANIAL. Methods for protecting network from islanding danger. *Journal of Engineering Research*. 2021, vol. 9, iss. 2, pp. 171–183. ISSN 2307-1885. DOI: 10.36909/jer.v9i2.9695.

[5] KIM, M.-S., R. HAIDER, G.-J. CHO, C.-H. KIM, C.-Y. WON and J.-S. CHAI. Comprehensive Review of Islanding Detection Methods for Distributed Generation Systems. *Energies*.

2019, vol. 12, iss. 5, pp. 1–21. ISSN 1996-1073. DOI: 10.3390/en12050837.

[6] REDDY, C. R. and K. H. REDDY. Islanding Detection Techniques for Grid Integrated Distributed Generation -A Review. *International Journal of Renewable Energy Research.* 2019, vol. 9, iss. 2, pp. 960–977. ISSN 1309-0127.

[7] HOSSEINZADEH, M. and F. R. SALMASI. Islanding Fault Detection in Microgrids—A Survey. *Energies.* 2020, vol. 13, iss. 13, pp. 1–28. ISSN 1996-1073. DOI: 10.3390/en13133479.

[8] TSHENYEGO, O., R. SAMIKANNU and B. MTENGI. Wide area monitoring, protection, and control application in islanding detection for grid integrated distributed generation: A review. *Measurement and Control.* 2021, vol. 54, iss. 5, pp. 585–617. ISSN 2051-8730. DOI: 10.1177/0020294021989768.

[9] RAMESH, V. and Y. K. LATHA. Performance improvement of grid connected PV system using new converter topologies. In: *2017 Second International Conference on Electrical, Computer and Communication Technologies (ICECCT).* Coimbatore: IEEE, 2017, pp. 1–5. ISBN 978-1-5090-3239-6. DOI: 10.1109/ICECCT.2017.8118002.

[10] KUMAR, P., V. KUMAR and B. TYAGI. Islanding detection for reconfigurable microgrid with RES. *IET Generation, Transmission* & *Distribution.* 2021, vol. 15, iss. 7, pp. 1187–1202. ISSN 1751-8695. DOI: 10.1049/gtd2.12095.

[11] RAYUDU, K., A. J. IAXMI, P. SOUMYA, R. PRADEEP and T. KOCHITO. Design of Controller for Transition of Grid Connected Microgrid to Island Mode. *Turkish Journal of Computer and Mathematics Education.* 2021, vol. 12, iss. 2, pp. 845–854. ISSN 1309-4653. DOI: 10.17762/turcomat.v12i2.1093.

[12] CHANAA, F., R. N. ZARRI, R. BENDAOUD, H. AMIRY, E. BAGHAZ, S. BOUNOUAR, B. ZOHAL, C. HAJJAJ, S. YADIR, A. EL-ABIDI and M. BENHMIDA. Islanding Detection Method of a Photovoltaic Installation Destined to Power a RLC Load and Integrated to LV Network. *International Journal of Intelligent Engineering* & *Systems.* 2021, vol. 14, iss. 4, pp. 299–311. ISSN 2185-3118. DOI: 10.22266/ijies2021.0831.27.

[13] PATHAN, E., S. A. ZULKIFLI, U. B. TAYAB and R. JACKSON. Small Signal Modeling of Inverter-based Grid-Connected Microgrid to Determine the Zero-Pole Drift Control with Dynamic Power Sharing Controller. *Engineering, Technology* & Applied Science Research. 2019,

vol. 9, iss. 1, pp. 3790–3795. ISSN 1792-8036. DOI: 10.48084/etasr.2465.

[14] CHUNG, P. D. Retaining of Frequency in Microgrid with Wind Turbine and Diesel Generator. *Engineering, Technology* & Applied Science Research. 2018, vol. 8, iss. 6, pp. 3646–3651. ISSN 1792-8036. DOI: 10.48084/etasr.2413.

[15] LIM, J. R., H. M. HWANG, W. G. SHIN, H.-J. SONG, Y.-C. JU, Y. S. JUNG, G. H. KANG and S. W. KO. Case Studies for Non-Detection of Islanding by Grid-Connected In-Parallel Photovoltaic and Electrical Energy Storage Systems Inverters. *Applied Sciences.* 2019, vol. 9, iss. 5, pp. 1–11. ISSN 2076-3417. DOI: 10.3390/app9050817.

[16] NAMDARI, F., M. PARVIZI and E. ROKROK. A Novel Passive Method for Islanding Detection in Microgrids. *Iranian Journal of Electrical and Electronic Engineering.* 2016, vol. 12, iss. 1, pp. 82–90. ISSN 1735-2827.

[17] DUTTA, S., P. K. SADHU, M. J. B. REDDY and D. K. MOHANTA. Shifting of research trends in islanding detection method - a comprehensive survey. *Protection and Control of Modern Power Systems.* 2018, vol. 3, iss. 1, pp. 1–20. ISSN 2367-0983. DOI: 10.1186/s41601-017-0075-8.

[18] LI, B., J. WANG, H. BAO and H. ZHANG. Islanding Detection for Microgrid Based on Frequency Tracking Using Extended Kalman Filter Algorithm. *Journal of Applied Mathematics.* 2014, vol. 2014, iss. 1, pp. 1–11. ISSN 1687-0042. DOI: 10.1155/2014/186360.

[19] YOUSSEF, T. A. and O. MOHAMMED. Adaptive SRF-PLL with reconfigurable controller for Microgrid in grid-connected and stand-alone modes. In: *2013 IEEE Power* & *Energy Society General Meeting.* Vancouver: IEEE, 2013, pp. 1–5. ISBN 978-1-4799-1303-9. DOI: 10.1109/PESMG.2013.6673028.

[20] GUPTA, P., R. S. BHATIA and D. K. JAIN. Active ROCOF Relay for Islanding Detection. *IEEE Transactions on Power Delivery.* 2016, vol. 32, iss. 1, pp. 420–429. ISSN 1937-4208. DOI: 10.1109/TPWRD.2016.2540723.

[21] CINTUGLU, M. H. and O. A. MOHAMMED. Islanding detection in microgrids. In: *2013 IEEE Power* & *Energy Society General Meeting.* Vancouver: IEEE, 2013, pp. 1–5. ISBN 978-1-4799-1303-9. DOI: 10.1109/PESMG.2013.6673041.

[22] SOMALWAR, R. S., D. A. SHINDE and S. G. KADWANE. Performance Evaluation of Voltage Ripple-Based Passive Islanding Detection Method for a Single-Phase

Utility-Connected Micro-Grid System. *IETE Journal of Research.* 2020. ISSN 0974-780X. DOI: 10.1080/03772063.2020.1844066.

[23] POURBABAK, H. and A. KAZEMI. Islanding detection method based on a new approach to voltage phase angle of constant power inverters. *IET Generation, Transmission & Distribution.* 2016, vol. 10, iss. 5, pp. 1190–1198. ISSN 1751-8695. DOI: 10.1049/iet-gtd.2015.0776.

[24] REDDY, C. R. and K. H. REDDY. An Efficient Passive Islanding Detection Method for Integrated DG System with Zero NDZ. *International Journal of Renewable Energy Research.* 2018, vol. 8, iss. 4, pp. 1994–2002. ISSN 1309-0127.

[25] FAQHRULDIN, O. N., E. F. EL-SAADANY and H. H. ZEINELDIN. A Universal Islanding Detection Technique for Distributed Generation Using Pattern Recognition. *IEEE Transactions on Smart Grid.* 2014, vol. 5, iss. 4, pp. 1985–1992. ISSN 1949-3061. DOI: 10.1109/TSG.2014.2302439.

[26] ABYAZ, A., H. PANAHI, R. ZAMANI, H. H. AL-HELOU, P. SIANO, M. SHAFIE-KHAN and M. PARENTE. An Effective Passive Islanding Detection Algorithm for Distributed Generations. *Energies.* 2019, vol. 12, iss. 16, pp. 1–19. ISSN 1996-1073. DOI: 10.3390/en12163160.

[27] GOUD, B. S., B. L. RAO and C. R. REDDY. Essentials for Grid Integration of Hybrid Renewable Energy Systems: A Brief Review. *International Journal of Renewable Energy Research.* 2020, vol. 10, iss. 2, pp. 813–830. ISSN 1309-0127.

[28] MUNUKUTLA, N. C., V. S. K. R. GADI and R. MYLAVARAPU. A Simplified Approach to Controlled Islanding of Power System. In: *2019 8th International Conference on Power Systems (ICPS).* Jaipur: IEEE, 2019, pp. 1–6. ISBN 978-1-7281-4103-9. DOI: 10.1109/ICPS48983.2019.9067725.

[29] SRIDEVI, J., V. U. RANI and B. L. RAO. Integration of Renewable DGs to Radial Distribution System for Loss Reduction and Voltage Profile Improvement. In: *2019 1st International Conference on Electrical, Control and Instrumentation Engineering (ICECIE).* Kuala Lumpur: IEEE, 2019, pp. 1–6. ISBN 978-1-7281-3939-5. DOI: 10.1109/ICECIE47765.2019.8974670.

[30] PRANAVI, K., P. L. REDDY and S. V. N. L. LALITHA. Optimal Sizing and Siting of BESS in Distribution Networks. *International Journal of Innovative Technology and Exploring Engineering.* 2019, vol. 8, iss. 6, pp. 1073–1078. ISSN 2278-3075.

[31] SRINIVASARAO, B., S. V. N. L LALITHA and Y. SREENIVASARAO. Evaluation of Closed-Loop-P.I.D, Fractional-Order-P.I.D and Proportional Resonant Controlled Micro-Grid-Schemes. *Journal of Computational and Theoretical Nanoscience.* 2019, vol. 16, iss. 5, pp. 2479–2487. ISSN 1546-1963. DOI: 10.1166/jctn.2019.7919.

[32] REDDY, C. R., K. H. REDDY K.H and K. V. S. REDDY. Recognition of Islanding Data for Multiple Distributed Generation Systems with ROCOF Shore Up Analysis. In: *Proceedings of the Second International Conference on SCI 2018.* Vijayawada: Springer, 2018, pp. 547–558. ISBN 978-981-13-1921-1. DOI: 10.1007/978-981-13-1921-1_54.

[33] RAJANNA, B. V. and K. S. SRIKANTH. Grid Connected Inverter for Current Control by Using Anti-Islanding Technique. *International Journal of Power Electronics and Drive Systems.* 2018, vol. 9, iss. 2, pp. 926–932. ISSN 2722-256X. DOI: 10.11591/ijpeds.v9.i2.pp926-932.

[34] KUMAR, M. K., C. VEERANJANEYULU and P. S. NIKHIL. Interfacing of Distributed Generation for Micro Grid Operation. *Journal of Advanced Researh in Dynamical and Control Systems.* 2018, vol. 10, iss. 4, pp. 472-477. ISSN 1943-023X.

[35] JYOTHI, K., K. S. SRIKANTH and H. S. JAIN. Control of Standalone and Grid Connected Distributed Energy Resource: A Review. *Journal of Advanced Researh in Dynamical and Control Systems.* 2018, vol. 10, iss. 12, pp. 1603–1615. ISSN 1943-023X.

[36] MAMANTHA, G., D. RANGASAI, S. AVINASH and M. NAVEEN. INTEGRATION OF SOLAR PV WITH GRID. *International Journal of Applied Engineering Research.* 2017, vol. 12, iss. 1, pp. 430–434. ISSN 1087-1090.

About Authors

Bangar Raju LINGAMPALLI (corresponding author) is currently working as Associate Professor in Swarna Bharati Institute of Technology, Khammam, Telangana State, India. He received his Bachelor of Engineering degree from Jawaharlal Nehru Technological University, Kakinada, Andhra Pradesh, India and M.Sc. (Engineering) in Power Systems from Calicut University. He has got 30 years of Industrial Experience in Power Plants, Oil and Gas, Petrochemical, Transmission, Distribution, Utilization. He has

published 11 International Scopus & WoS Indexed Journal Papers. He is a Life Member of ISTE (Indian Society for Technical Education) and IE (Institute of Engineers, India). He is currently pursuing his Ph.D. degree from Koneru Lakshmaiah Educational Foundation (Deemed to be University), Greenfields, 522502 Vaddeswaram, Andhra Pradesh, India. His areas of interest are Power System Protection, Distributed Generation and Microgrids.

Subba Rao KOTAMJARU is presently Principal, College of Engineering and Professor of Electrical and Electronics Engineering Department of Koneru Lakshmaiah Educational Foundation (Deemed to be University), Greenfields, 522502 Vaddeswaram, Andhra Pradesh, India. He received his Ph.D. degree from Koneru Lakshmaiah Educational Foundation (Deemed to be University), Greenfields, 522502 Vaddeswaram, Andhra Pradesh, India, M.Tech. from Coimbatore Institute of Technology, Coimbatore and B.Tech. from Dayalbagh University, Agra. He has achieved 10 times best teacher award. He is a Life Member of ISTE and Indian Society for Quality. He has published both national and international papers and a book. His areas of interest are Power Electronics, Power Systems, Microgrids and Security Systems.

Appendix A
List of Abbreviations

- *abc* to *dq*0 – 3-phase instantaneous rotating A.C. quantities to 2-phase rotating DC quantities - also called as "Park Transformation *abc* to *dq* axis",

- *j* – is an operator which rotates the vector by 90 degrees in anti-clockwise direction,

- Δ – incremental value,

- Hz – hertz – cycles per second (unit of frequency),

- kW – kilowatts (active power - P),

- kVAR – kilo Volt Amperes Reactive (reactive power - Q),

- p.u. – per unit,

- % – percentage,

- Φ – phase angle (unit degrees or radians),

- du/dt – differentiator (unit u per second),

- k_p/k_i – current controller proportional gain/integral gain.